Filling the Gap in Extended Metal Atom Chains: Ferromagnetic Interactions in a Tetrairon(II) String Supported by Oligo-α-pyridylamido Ligands / Nicolini, A., Galavotti, R., Barra, A., Borsari, M., Caleffi, M., Luo, G., Novitchi, G., Park, K., Ranieri, A., Rigamonti, L., Roncaglia, F., Train, C., Cornia, A.. - In: INORGANIC CHEMISTRY. - ISSN 0020-1669. - 57:9(2018), pp. 5438-5448. [10.1021/acs.inorgchem.8b00405]

Filling the gap in Extended Metal Atom Chains: Ferromagnetic Interactions in a Tetrairon(II) String Supported by Oligo-α-pyridylamido Ligands

*Alessio Nicolini,[a,b] Rita Galavotti,[a] Anne-Laure Barra,[c] Marco Borsari,[a] Matteo Caleffi,[a] Guangpu Luo,[d] Ghenadie Novitchi,[c] Kyungwha Park,[d] Antonio Ranieri,[e] Luca Rigamonti,[a] Fabrizio Roncaglia,[a] Cyrille Train[c] and Andrea Cornia[a]**

[a]Department of Chemical and Geological Sciences, University of Modena and Reggio Emilia & INSTM, I-41125 Modena, Italy

[b]Department of Physics, Informatics and Mathematics, University of Modena and Reggio Emilia, I-41125 Modena, Italy

[c]Laboratoire National des Champs Magnétiques Intenses-CNRS, Université Joseph Fourier, F-38042 Grenoble Cedex 9, France

[d]Department of Physics, Virginia Tech, Blacksburg, Virginia, United States 24061

[e]Department of Life Sciences, University of Modena and Reggio Emilia, I-41125 Modena, Italy

ABSTRACT

The string-like complex $[Fe_4(tpda)_3Cl_2]$ (H_2tpda = N^2,N^6-di(pyridin-2-yl)pyridine-2,6-diamine) (**2**) was obtained as the first homometallic extended metal atom chain based on iron(II) and oligo-α-pyridylamido ligands. The synthesis was performed in strictly anaerobic and anhydrous conditions using dimesityliron, $[Fe_2(Mes)_4]$ (HMes = mesitylene) (**1**) as both an iron source and a deprotonating agent for H_2tpda. The four lined-up iron(II) ions in the structure of **2** (Fe···Fe = 2.94-2.99 Å, Fe···Fe···Fe = 171.7-168.8°) are wrapped by three doubly-deprotonated twisted ligands and the chain is capped at its termini by two chloride anions. The spectroscopic and electronic properties of **2** were investigated in dichloromethane by UV-Vis-NIR absorption spectroscopy, ^{1}H-NMR spectroscopy and cyclic voltammetry. The electrochemical measurements showed four fully resolved, quasi-reversible one-electron redox processes, implying that **2** can adopt five oxidation states in a potential window of only 0.8 V. Direct current magnetic measurements indicate dominant ferromagnetic coupling at room temperature, although the ground state is only weakly magnetic. Based on Density Functional Theory and Angular Overlap Model calculations, this magnetic behavior was explained as being due to two pairs of ferromagnetically-coupled iron(II) ions ($J = -21$ cm^{-1} using $J\hat{\mathbf{S}}_i \cdot \hat{\mathbf{S}}_j$ convention) weakly antiferromagnetically coupled with each other. Alternating-current susceptibility data in the presence of a 2 kOe dc field and at frequencies up to 1.5 kHz revealed the onset of slow magnetic relaxation below 2.8 K, with an estimated energy barrier $U_{\mathrm{eff}}/k_{\mathrm{B}}$ = 10.1(1.3) K.

INTRODUCTION

EMACs (Extended Metal Atom Chains) constitute a wide class of polynuclear metal complexes containing three to eleven metal centers lined up in a string by an array of deprotonated oligo-α-pyridylamine or related ligands.[1-3] In these materials, which may be homo- or hetero-metallic, homo- or heterovalent, the arrangement of donor atoms often promotes the formation of metal-metal bonds.[1] EMACs were consequently investigated as analogues of macroscopic wires in molecular electronics.[4-7] Recently, EMACs have attracted renewed interest after some of us reported that pentachromium(II) complex [$Cr_5(tpda)_4Cl_2$] shows a directionally-bistable magnetic moment in its $S = 2$ ground state at low temperature.[8] The shorter complex [$Cr_3(dpa)_4Cl_2$]·CH_2Cl_2 and its Mo_2Cr and W_2Cr heterometallic analogues were subsequently found to display similar properties.[9,10]

Homometallic iron-based EMACs are particularly appealing synthetic targets in molecular magnetism owing to the large spin and magnetic anisotropy of high-spin iron(II).[11] In addition, low-valent polyiron species with short metal-metal separations (or even true metal-metal bonds) may exhibit strong ferromagnetic interactions and high-spin states persistent to room temperature.[12-18] This counterintuitive result is attributed to the occurrence of a manifold of delocalized d-type molecular orbitals closely-spaced in energy and populated according to Hund's rule.[14-18] The triiron(II) EMAC [$Fe_3(dpa)_4Cl_2$] was indeed theoretically predicted to have short Fe···Fe distances (2.53 Å) and an $S = 6$ ground state;[19] unfortunately, such a species has so far escaped isolation, although iron(II) was incorporated into structurally-similar heterometallic EMACs.[20-24] To the best of our knowledge, the only homometallic iron-based EMAC was reported by Cotton *et al.* in 1998 and is a homoleptic trinuclear complex of *N*,*N*′-di(2-pyridyl)formamidinato ligands. Although it contains no metal-metal bonds (Fe···Fe 2.78 Å), its room-temperature magnetic moment is well above the expected value for three uncoupled high-spin centers, hinting to strongly ferromagnetic interactions.[25]

Here, we demonstrate that homometallic iron(II) EMACs can be assembled by using oligo-α-pyridylamines, the family of ligands of most widespread use in EMAC chemistry. The key to success was utilizing dimesityliron, [$Fe_2(Mes)_4$] (**1**),[26,27] as both an iron source and a deprotonating agent for H_2tpda. The product, [$Fe_4(tpda)_3Cl_2$] (**2**), defines a new structural type in EMAC chemistry, with four divalent metal ions helically wrapped by three tpda^{2-} ligands. As predicted by DFT calculations the complex shows dominant ferromagnetic interactions at room temperature, with two pairs of ferromagnetically-coupled iron(II) ions exhibiting weak antiferromagnetic interactions with each other.

EXPERIMENTAL SECTION

Materials and methods. Because iron amides are exceedingly air sensitive, all operations were carried out in an MBraun UniLAB glovebox under an inert and controlled dinitrogen atmosphere continuously purified over molecular sieves and a copper catalyst (H_2O and O_2 < 1 ppm). All solvents were anhydrous and of commercial origin (except for Et_2O, which was distilled from its sodium benzophenone ketyl solution before use); they were deoxygenated through three *freeze-pump-thaw* cycles and stored over 4A molecular sieves.[28] Compounds **1**[26,27] and $Fe_4Cl_8·6THF$[29] were prepared according to well-established literature methods. H_2tpda was obtained by refluxing 2,6-diaminopyridine with 2-fluoropyridine and LiH in toluene/pyridine, following a recently-reported high-yield procedure.[30] Elemental analysis was performed using a ThermoFisher Scientific Flash 2000 analyzer. ESI-MS measurements were made on a 6310A Ion Trap LC-MS(n) instrument (Agilent Technologies) by direct infusion of dichloromethane solutions. The electronic spectra were recorded on solutions of **2** in dichloromethane using a UV-Vis-NIR Jasco V-570 spectrometer and a quartz cuvette sealed with an air-tight teflon cap (optical path length: l = 0.1 cm). The spectrum of the H_2tpda ligand was also measured before and after the addition of excess ^{t}BuOK. Since solutions of H_2tpda and ^{t}BuOK in dichloromethane gave time-dependent spectra, tetrahydrofuran was used as solvent. Room temperature ^{1}H-NMR spectrum was recorded on a CD_2Cl_2 solution of **2** using a valved 5 mm NMR tube and a Bruker Avance400 FT-NMR spectrometer (400.13 MHz). The chemical shifts are expressed in ppm downfield from Me_4Si as external standard, by setting the residual ^{1}H signal of CD_2Cl_2 at 5.32 ppm.

Synthesis of $[Fe_4(tpda)_3Cl_2]\cdot 2.6CH_2Cl_2\cdot 0.84Et_2O$ (**2**$\cdot$2.6$CH_2Cl_2\cdot$0.84Et_2O). A suspension of H_2tpda (97.9 mg, 0.372 mmol) in toluene (3.6 mL) was added dropwise to a red solution of **1** (109.4 mg, 0.1859 mmol) in toluene (4 mL) under stirring. During the addition of the ligand the reaction mixture turned into a brown suspension. $Fe_4Cl_8\cdot 6THF$ (22.0 mg, 0.0937 mmol of Fe) was then added to afford an orange suspension. The reaction mixture was carefully heated to the reflux temperature for 2 h 45 min and subsequently cooled down to room temperature (an ESI-MS spectrum of the reaction mixture is presented in Figure S1). The brown-orange solid was separated from the dark red liquid phase by centrifugation and repeatedly extracted with CH_2Cl_2 (9 × 3 mL) to give an orange solution. Slow diffusion of diethyl ether (1.4 times by volume) into the CH_2Cl_2 solution afforded dark-red prisms of the product (Figure S2). The crystals were separated from a powdery residue by flotation and stored at –80 °C in flame-sealed quartz tubes containing their mother liquor. After magnetic measurements, the product was dried in vacuum to give an orange powder (27 mg, 27%). All subsequent characterizations, except for elemental analysis, were performed with strict exclusion of dioxygen and water. For elemental analysis, the sample had to be briefly exposed to the air, whereupon it immediately darkened due to reaction with dioxygen and/or water. Although incorporation of oxygen may explain the lower than calculated C,H,N content (see below), the reliability of elemental analysis data for **2** is limited. The homogeneity of bulk samples was inferred from ^{1}H-NMR spectra (see text) and from the X-ray analysis performed on *eight* single crystals taken from the same or different syntheses, which invariably gave the same unit-cell parameters. Anal. Calcd for **2**: C, 50.13; H, 3.09; N, 19.49; for **2**+1.37O_2: C, 48.17; H, 2.96; N, 18.73. Found: C, 48.07; H, 3.05; N, 18.96. ESI-MS (*m*/*z*): 986.2 ($[Fe_3(tpda)_3Cl]^+$, 100); 1030.0 ($[Fe_3(tpda)_3Br]^+$, 13). UV-Vis-NIR (CH_2Cl_2, $2\cdot 10^{-4}$ M): λ_{max} (ε) = 288 nm ($4.49\cdot 10^4$ M^{-1} cm^{-1}), 374 nm ($4.13\cdot 10^4$ M^{-1} cm^{-1}), 450 nm (sh). ^{1}H-NMR (CD_2Cl_2, 400.13 MHz): δH (ppm) = 5.94 (6H, s), 10.27 (3H, s, H*a*), 10.83 (6H, s), 62.55 (6H, s), 82.04 (6H, s), 123.2 (6H, s).

X-ray Crystallography. The single-crystal X-ray structure determination on **2**$\cdot$2.6$CH_2Cl_2$$\cdot$0.84$Et_2O$ was carried out at 115(2) K on a Bruker-Nonius X8APEX diffractometer equipped with Mo-Kα generator, area detector and Kryoflex liquid nitrogen cryostat. Crystals of the compound and a small amount of mother liquor were transferred out of the glovebox using a Schlenk flask. The Schlenk was then opened under fast dinitrogen flux and the selected crystal was covered with epoxy glue, rapidly mounted on the tip of a glass capillary and directly transferred to the cold dinitrogen flux of the cryostat. Data collection and reduction were carried out using APEX2[31] and SAINT[31] softwares, respectively, while absorption correction was applied with SADABS.[31] The structure was solved and refined on F_o^2 by standard methods, using SIR92[32] and SHELXL-2014/7[33] programs implemented in the WINGX v2013.3 suite.[34] All non-hydrogen atoms were refined anisotropically, unless otherwise noted, while hydrogen atoms were added in idealized positions, allowed to ride on the parent carbon atoms and treated isotropically with $U(\mathrm{H}) = 1.2U_{\mathrm{eq}}(\mathrm{C})$ for aromatic and methylene hydrogens and $U(\mathrm{H}) = 1.5U_{\mathrm{eq}}(\mathrm{C})$ for methyl hydrogens.

A total of 2.6 and 0.84 CH_2Cl_2 and Et_2O molecules, respectively, were located in the lattice per tetrairon(II) unit. Two interstitial CH_2Cl_2 molecules with full and ~0.44 occupancies, respectively, were subject to unrestrained refinement. The remaining interstitial solvent molecules were extensively disordered and overlapping, so that restraints had to be applied to their geometry and displacement parameters. The CH_2Cl_2 and Et_2O molecules with the largest occupancy were used as structural references for geometrical restraints, with esd values of 0.01 and 0.02 Å for 1,2- and 1,3-distances, respectively. In the reference Et_2O molecule, O–C and C–C bond lengths were also restrained to be equal within 0.01 Å. All atoms in the minority Et_2O component and a few poorly-resolved C atoms of CH_2Cl_2 molecules were treated isotropically. Enhanced rigid bond restraints[35] were applied to bonded anisotropic atoms (RIGU instruction with esd values of 0.004 Å^2 for both 1,2- and 1,3-distances). Crystal data and refinement parameters are gathered in Table 1 while interatomic distances and angles are presented in Table 2 (more exhaustive listings are available in Table S1 and S2).

Electrochemistry. A Potentiostat/Galvanostat mod. PARSTAT 2273 (Princeton Applied Research, Oak Ridge, USA) was used to perform CV. Experiments were carried out at different scan rates ($v = 0.02 - 5$ V s^{-1}) using a cell for small volume samples (0.5 mL). A 1 mm-diameter GC disk (PAR), a Pt wire and an Ag wire were used as working, counter, and quasi-reference electrode, respectively. The GC electrode was cleaned following a procedure which ensures a suitable and reproducible surface for ET studies.[36] For all experiments, the potential of the quasi-reference electrode was calibrated against the ferricenium/ferrocene redox couple (in dichloromethane, $E° = 0.460$ V against the KCl SCE).[37] All the reported potential values are referred to ferricenium/ferrocene redox couple. Since the complex degrades quickly in the presence of O_2 or H_2O, all the experiments were carried out in the above-described MBraun UniLAB glovebox under dinitrogen at –10 °C. Dichloromethane/0.1 M TBACl or $TBABF_4$ was used as electrolyte support solution. To reduce the amount of water, TBACl ($TBABF_4$) was recrystallized twice from acetone/Et_2O (EtOH/Et_2O). The filtered solids were washed with Et_2O and dried under vacuum.[28] The typical complex concentration was 0.2 mM. To minimize the ohmic drop between the working and the reference electrodes, careful feedback correction was applied. The formal potential value ($E°'$) corresponding to each ET process was calculated as the semi-sum of the cathodic and anodic peak potentials, $E°'=(E_{pc}+E_{pa})/2$. The dependence of $\Delta E_p = E_{pa} - E_{pc}$ on v allows to obtain the standard heterogeneous ET rate constant k_{ET},[38] which is the ET rate constant measured at the formal potential $E°'$. The experiments were repeated at least five times and the k_{ET} values obtained were found to be reproducible within 6%.

Magnetic measurements. Magnetic measurements were made on an MPMS5 Quantum Design instrument. A sample of **2**·2.6CH_2Cl_2·0.84Et_2O was introduced in a flame-sealed quartz tube together with a small amount of mother liquor (a mixture of CH_2Cl_2 and Et_2O 71:29 *w*/*w*) to preserve crystallinity and avoid field-induced torqueing at low temperature. The mass of the sample and of the mother solution were determined after magnetic measurements were completed: 14.08 mg of desolvated **2** (corresponding to 17.78 mg of **2**$\cdot$2.6$CH_2Cl_2\cdot$0.84Et_2O) and 30.96 mg of mother solution. The diamagnetic contributions of the sample and of the mother solution were evaluated using Pascal's constants[39] and the specific susceptibilities of the solvents, respectively, while the magnetic response of the empty quartz tube was separately measured. Magnetization (M) measurements were carried out at $H = 1$ kOe between 2.0 and 300 K and the magnetic susceptibility was calculated as $\chi = M/H$. The field dependence of the magnetization was also measured up to 50 kOe at 2, 3, 4 and 5 K. AC measurements were performed using a 3.0 Oe oscillating field with frequencies in the 1−1500 Hz range. EPR experimental details are available in the SI.

Theoretical calculations. Ligand field calculations were carried out within the AOM, using the AOMX program package.[40] Experimental atomic coordinates for the terminal Fe1(N1,N2,N3,Cl1) and Fe4(N13,N14,N15,Cl2) chromophores were either used directly or averaged to C_{3v} symmetry in order to evaluate ligand-field splittings. Ligand-field parameters that account for σ and π interactions were based on previous work[41] and in particular on structural and spectroscopic literature data for *trans*-[Fe(py)$_4$Cl$_2$] and *trans*-[Fe(py)$_4$(NCS)$_2$], which feature a tetragonally-elongated octahedral geometry.[42-44] The actual ligand field parameters used in the calculations were obtained from the above-reported literature values by assuming a r^{-6} dependence on metal-donor distance r. Interelectronic repulsion parameters were set at $B = 850$ cm^{-1}, $C = 3100$ cm^{-1} (both ca. 20% lower than the free-ion value[45]), the effective spin-orbit coupling constant was set at $\zeta_{3d} = 350$ cm^{-1} and a unitary and isotropic orbital reduction factor (k) was used[44] (see Supporting Information for details). AOM calculations on Fe2 and Fe3 ions were directly based on experimental atomic coordinates of Fe2(N4,N5,N6,N7,N8) and Fe3(N8,N9,N10,N11,N12) chromophores and on the same B, C, ζ_{3d} and k values as above. The ligand-field e_σ(N) parameters were estimated from Fe–N distances treating all donors as py-type N donors for simplicity and using the same r^{-6} power law described above.

We carried out DFT calculations on **2** by using NRLMOL[46-48] and VASP,[49,50] within PBE GGA exchange-correlation functional.[51] For NRLMOL, we considered all electrons and generally contracted Gaussian basis sets (better than triple zeta) for all elements, whereas for VASP we employed plane-wave basis sets with energy cutoff of 400 eV with PAW pseudopotentials.[52,53] The experimental geometry has been used. For the bonding analysis, we employed an on-site Coulomb repulsion term, $U = 2$, for the Fe *d* orbitals, including self-consistent spin-orbit coupling to the lowest-energy state, i.e. up-up-down-down spin configuration, in VASP.

RESULTS AND DISCUSSION

Synthesis and solution studies. The key to success in the synthesis was utilizing dimesityliron, $[Fe_2(Mes)_4]$ (**1**),[26,27] as the main iron source. The Mes^- ligand in this extremely air-sensitive and thermally-labile compound is a very strong base, allowing to access iron amides with formation of mesitylene as the only byproduct of the reaction.[54,55] Refluxing **1** with $Fe_4Cl_8{\cdot}6THF$ (0.5 equivs of Fe)[29] and H_2tpda (2 equivs) in toluene under strict exclusion of dioxygen and moisture resulted in an orange precipitate. This solid was extracted with CH_2Cl_2 and recrystallized by vapor diffusion of Et_2O, reproducibly affording dark-red prisms of $[Fe_4(tpda)_3Cl_2]{\cdot}2.6CH_2Cl_2{\cdot}0.84Et_2O$ (**2**$\cdot 2.6CH_2Cl_2{\cdot}0.84Et_2O$) in 25-30% yield (Figure S2). Notice that the used molar ratios imply a 25-% understoichiometric amount of $Fe_4Cl_8{\cdot}6THF$, since they were tuned for the preparation of $[Fe_5(tpda)_4Cl_2]$, which turned out to be synthetically inaccessible. Alternative routes widely used in EMACs chemistry, like prolonged heating of metal dichloride/H_2tpda/^{t}BuOK[2] or metal diacetate/H_2tpda[56] mixtures in refluxing naphthalene, failed to produce any tractable solid.

The ESI-MS spectrum of **2**·2.6CH_2Cl_2·0.84Et_2O crystals dissolved in dichloromethane (Figure S3) exhibits a strong peak at m/z = 986.2 and a much weaker signal at m/z = 1030.0. The reaction mixture before workup yields the same peaks (Figure S1), neither of which corresponds to the molecular ion signal. Rather, they have the correct isotopic pattern for the mixed-valent species $[Fe_3(tpda)_3Cl]^+$ and $[Fe_3(tpda)_3Br]^+$, respectively (bromide ions are trace residuals from the preparation of **1**).

The electronic spectra of the free H_2tpda ligand in dichloromethane[57] (tetrahydrofuran) are dominated by two intense absorptions at 262 (262) and 332 (336) nm, assigned to $\pi \rightarrow \pi^*$ transitions.[58] These bands undergo a large red shift to 320 and 390 nm upon ligand deprotonation by addition of excess ^{t}BuOK in tetrahydrofuran (Figure S4). A qualitatively similar shift is observed in the electronic spectrum of **2** in dichloromethane, which shows two intense absorption bands at 288 and 374 nm along with a weaker shoulder at ~448 nm, which conveys a light yellow-brown color to the solution (Figure S4). Upon admission of oxygen to the cuvette, the spectrum rapidly evolves and the final profile is superimposable to the spectrum of H_2tpda.

Since neither ESI-MS nor UV-Vis-NIR spectroscopy directly support the stability of **2** in dichloromethane solution, we recorded an ^{1}H-NMR spectrum in CD_2Cl_2 (Figure 1). We found six well-resolved singlets covering a chemical shift range exceeding 100 ppm, indicating strong interaction with paramagnetic centers in **2**. Comparison with the ^{1}H-NMR spectrum of H_2tpda[30] shows that all signals except *I* undergo downfield paramagnetic shifts. Both the number of observed resonances and their 2:1:2:2:2:2 intensity ratios (in order of increasing chemical shift) require that only 6 of the 11 hydrogen atoms in each ligand's molecule are chemically inequivalent. Overall, experimental results are in accordance with the solid state structure assuming that the unsymmetric binding of $tpda^{2-}$ ligands is averaged out in solution, in such a way that the maximum possible symmetry for a helical structure (D_3) is detected over NMR timescale (see below). A pentachromium(II) EMAC in dichloromethane solution has been similarly found to display its maximum possible symmetry (D_4) on the timescale of NMR experiment, although the solid state structure is much less symmetric.[30] Even if a complete assignment of protons pattern is not possible at this stage of investigation, the intensity ratios suggest that signal *II* corresponds to H*a*.

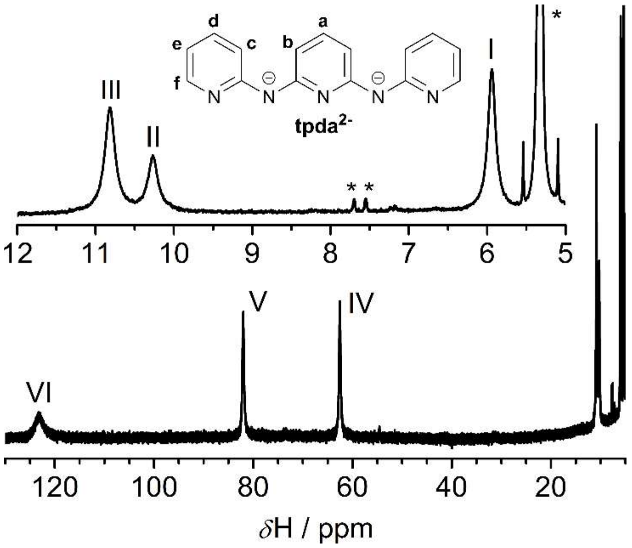

Figure 1. Room-temperature ^{1}H-NMR spectrum of **2** in CD_2Cl_2 (400.13 MHz). The inset shows an expanded view of the area between 12 and 5 ppm, and the molecular structure of tpda^{2-} (with the hydrogen labelling scheme). Peaks marked with an asterisk arise from residual protons in CD_2Cl_2 (5.32 ppm) and from so far unidentified impurities (7.55 and 7.70 ppm). Processing parameters (TopSpin 3.5 pl 7): SI = TD, LB = 1.00 Hz. The spectral region between 5 and 0 ppm contains no peaks from the compound and is available in Figure S5.

X-ray structure. A single-crystal X-ray diffraction study at 115(2) K (Table 1) evidenced that **2**$\cdot 2.6CH_2Cl_2 \cdot 0.84Et_2O$ contains tetrairon string-like complexes wrapped by three doubly-deprotonated *all-syn* H_2tpda ligands and capped at their termini by two chloride ions (selected bond distances and angles are gathered in Table 2). Consistent with this formulation, Bond-Valence Sum calculations[59] confirmed that the four metal ions are in a +2 oxidation state (Table S3).

Table 1. Crystal data and refinement parameters for **2**·$2.6CH_2Cl_2$·$0.84Et_2O$

Formula	$C_{50.95}H_{46.58}Cl_{7.20}Fe_4N_{15}O_{0.84}$
T (K)	115(2)
Crystal System	monoclinic
Space group	$P2_1/c$
a (Å)	19.3496(11)
b (Å)	16.2825(10)
c (Å)	18.5919(10)
α (°)	90.000
β (°)	104.504(2)
γ (°)	90.000
V (Å^3)	5670.9(6)
Z	4
ρ_{calc} (g cm^{-3})	1.594
θ_{min} / θ_{max} (°)	2.992 / 27.017
No. collected/indep. reflections	49632/12243
R_{int}	0.0461
Parameters/restraints	784/64
$R1$, $wR2$	0.0685, 0.1185
$R1$, $wR2$ [$I > 2\sigma(I)$]	0.0447, 0.1056
GOF	1.084
Largest diff. peak / hole (e Å^{-3})	1.069 / –0.638

As shown in Figure 2, all five nitrogen donors of the organic ligands are coordinated to the metals. The metal centers are arranged in a slightly helical zig-zag fashion (Fe···Fe···Fe = 171.7-168.8°, Fe···Fe···Fe···Fe torsion angle = 173.0°) and Fe···Fe distances range from 2.94 to 2.99 Å. DFT calculations show that the HOMO (HOMO–1) level arises mainly from Fe1 (Fe4) only, which indicates that no metal-metal bonds are formed. Fe···Fe distances are however shorter than in diiron(II) complexes containing lower congeners of tpda^{2-}, like [$Fe_2Cl(dpa)_3$] (**3**),[55] [$Fe_2(Mes)_2(dpa)_2$] (**4**)[55] and [$Fe_2(dpa)_2(hmds)_2$] (**5**),[60] where iron ions are 3.104(2), 3.043(1) and 3.3609(1) Å apart, respectively, but longer than in the homoleptic triiron(II) complex described by Cotton *et al.*.[25]

Table 2. Interatomic distances [Å] and angles [°] for **2**·2.6CH_2Cl_2·0.84Et_2O

Fe(1)–Fe(2)	2.9907(6)	Fe(2)–Fe(3)	2.9641(6)
Fe(3)–Fe(4)	2.9414(6)	Fe(1)–N(1)	2.088(3)
Fe(1)–N(2)	2.092(3)	Fe(1)–N(3)	2.087(3)
Fe(1)–Cl(1)	2.3860(8)	Fe(2)–N(4)	2.113(3)
Fe(2)–N(5)	2.014(3)	Fe(2)–N(6)	2.012(3)
Fe(2)–N(7)	2.187(3)	Fe(2)–N(8)	2.4557(25)
Fe(3)–N(8)	2.5248(26)	Fe(3)–N(9)	2.231(3)
Fe(3)–N(10)	2.031(3)	Fe(3)–N(11)	2.014(3)
Fe(3)–N(12)	2.104(3)	Fe(4)–N(13)	2.085(3)
Fe(4)–N(14)	2.079(3)	Fe(4)–N(15)	2.069(3)
Fe(4)–Cl(2)	2.3576(9)		
Cl(1)–Fe(1)–Fe(2)	177.27(3)	Fe(1)–Fe(2)–Fe(3)	171.67(2)
Fe(4)–Fe(3)–Fe(2)	168.76(2)	Cl(2)–Fe(4)–Fe(3)	178.92(3)

As a consequence of steric interaction between pyridyl β hydrogens, the tpda^{2-} ligands adopt a helical arrangement around the metal ion chain. The molecule is thus chiral, but both enantiomers are present in the crystal in 1:1 proportions because of the centrosymmetric space group. The pitch of the structure, as defined by the average N–M···M–N torsion angle involving the two terminal metal ions and the N atoms of the same tpda^{2-} ligand, averages to 105°. It is thus distinctly larger than found in the Cr_5,[61] Co_5[62] and Ni_5[63] analogues containing four tpda^{2-} ligands (81, 89 and 90°, respectively).

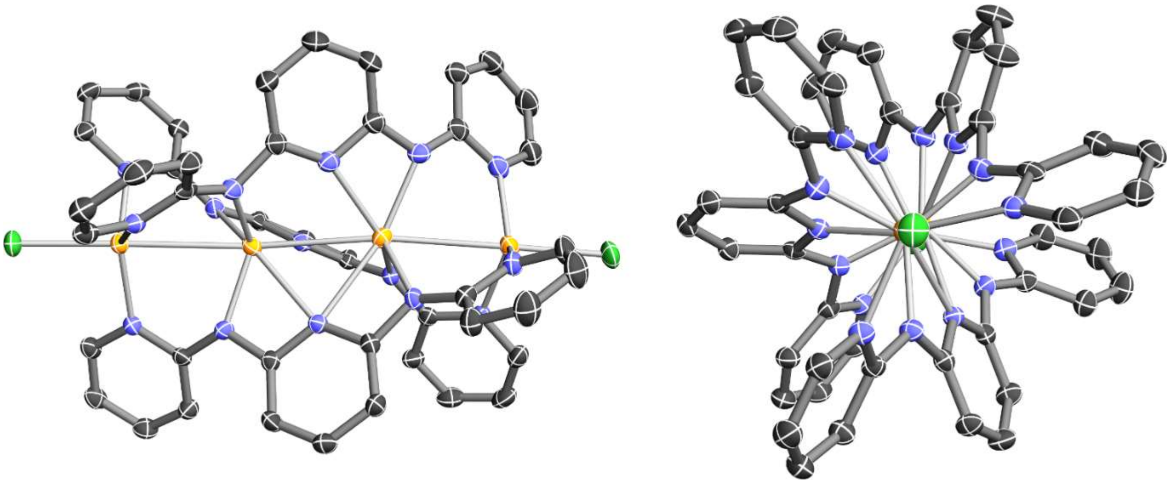

Figure 2. Molecular structure of **2**, viewed approximately normal to the metal axis (left) and along it (right). Color code: orange = Fe, dark grey = C, blue = N, green = Cl. Lines connecting iron(II) ions are included for a better representation and do not correspond to chemical bonds. Hydrogen atoms are omitted for clarity and thermal ellipsoids are drawn at 60% probability level.

The terminal iron ions (Fe1 and Fe4) are tetracoordinated by three pyridyl N atoms and by one chloride ligand to give a distorted trigonal-pyramidal geometry (Fe-N = 2.07-2.09 Å, Fe-Cl = 2.36-2.39 Å, Cl-Fe-N = 95.2-98.3°, N-Fe-N = 111.9-125.4°). A similar coordination environment was previously found for one of the iron(II) centers in complex $[Fe_2(py_3tren)Cl]$ (**6**).[16] The inner iron ions (Fe2 and Fe3) have a much less regular pentacoordinated environment (Figure 3). Each of them has the shortest coordination bonds with three amide N donors (Fe–N = 2.01-2.11 Å) and has an additional contact with one of the central pyridyl rings (Fe–N = 2.19-2.23 Å). In this way, two tpda^{2-} ligands form four-membered chelate rings through their central pyridyl moieties (N7 and N9) and one of the neighboring amide groups (N4 and N12). The central nitrogen of the third tpda^{2-} ligand (N8) is engaged in long (2.46-2.52 Å) contacts with both Fe2 and Fe3. Because of the pronounced binding asymmetry of two over four tpda^{2-} ligands, complex **2** in the solid state does not have the maximum symmetry achievable for this type of helical structure (D_3) but displays idealized twofold symmetry approximately normal to the metal chain.

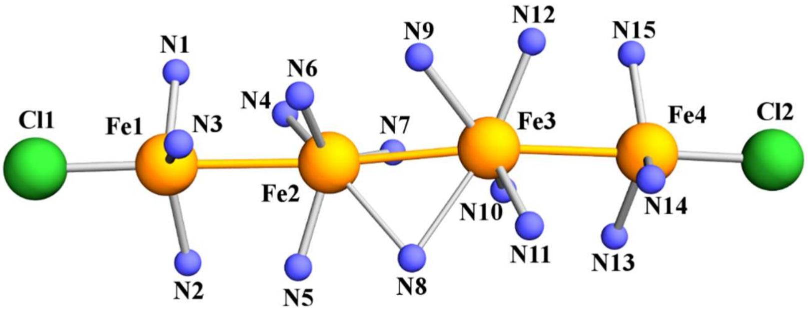

Figure 3. Coordination environment of the four metal ions in **2**, with the atom labeling scheme and the same color code as in Figure 2. Lines connecting iron(II) ions are included for a better representation and do not correspond to chemical bonds.

Beside representing a new structural type in EMAC chemistry, complex **2** qualifies as the first iron-based EMAC supported by oligo-α-pyridylamido ligands, although it contains one metal *less* than expected from ligand's structure. Interestingly, a similar situation holds with tridentate dpa^{-}, which has so far afforded diiron complexes only. Two of them (**3** and **4**) were obtained as **3**$[Fe_4O(dpa)_6]\cdot 3C_7H_8$ and **4**$\cdot C_7H_8$ by treating **1** with excess Hdpa in hot toluene.[55] The latter compound represents the main product of the reaction, with oxide and chloride ions in **3** being adventitious. In early work, from Li(dpa) and $FeCl_2$ in THF/toluene Cotton *et al.* obtained only the μ_4-oxo centered tetrahedral complex $[Fe_4O(dpa)_6]$, again containing adventitious oxide.[64] A third complex (**5**) structurally similar to **4** was prepared starting from $Fe(hmds)_2$ as an iron source.[60] Since both tri- and pentaruthenium(II) EMACs have been reported,[65] the paucity of iron-based strings most likely arises from the high tendency of Fe^{2+} toward oxidation and hydrolysis in the reaction conditions.

Electrochemistry. The CV curve for the complex in dichloromethane is shown in Figure 4. It consists of four consecutive oxidation peaks with the corresponding reduction counterparts (hereafter indicated as signals I, II, III, and IV at increasing potential values). The CV curves show a poor reproducibility when $TBABF_4$ is used as base electrolyte. In fact, after few minutes both the cathodic and anodic peaks decrease and broaden and new signals appear. After about one hour, only two new couples of persistent cathodic and anodic peaks can be observed. On the contrary, using TBACl as base electrolyte the CV signals are the same as initially observed in the presence of $TBABF_4$, are stable and do not change with time. These different behaviors could be related to solvolysis processes involving, in particular, the detachment of the terminal chloride ligands. In the presence of an excess of Cl^- in the solution due to the base electrolyte, this process does not occur or is extremely slow.

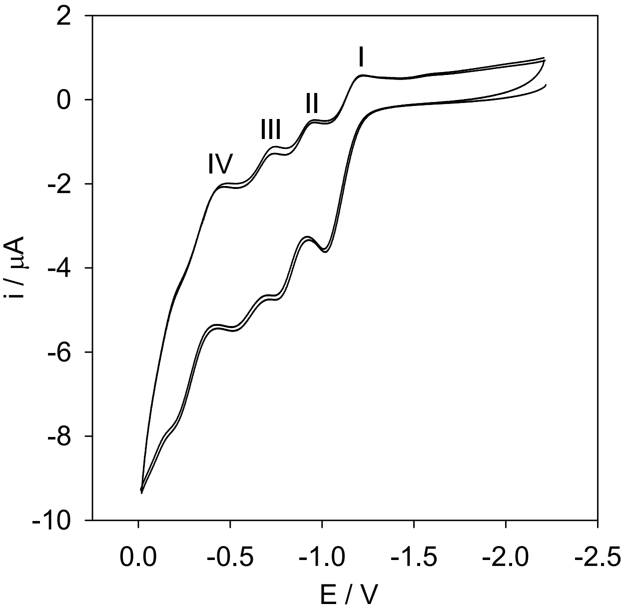

Figure 4. Cyclic voltammogram of **2**. Working electrode: glassy carbon, 0.1 M TBACl in dichloromethane (scan rate $v = 0.05$ V/s; reference: Fc^+/Fc).

The peak-to-peak separation of each signal couple increases with the potential scan rate (v) and varies for the different signal couples, in particular it increases from signal I to IV. The peak currents of all the signals are proportional to the square root of v. This means that the electrochemistry of the complex consists in four quasi-reversible, diffusion-controlled redox processes. The formal potential values $E°'$ and the standard heterogeneous ET rate constants k_{ET} associated with the redox processes are reported in Table 3. The CV curves obtained by stopping the scan after each anodic peak strictly resemble (in terms of calculated $E°'$, peak-to-peak separation and peak currents) the traces recorded in a single scan involving all four quasi-reversible signals. This result indicates that no appreciable chemical reactions or structural rearrangements affect the observed ET processes (at least over the time scale of the electrochemical measurement).

Complex **2** shows a peculiar redox behaviour since five oxidation states (four quasi-reversible ET processes) are observed in a potential window of only 0.8 V. The fully resolved, quasi-reversible one-electron redox processes corresponding to successive oxidations suggest the presence of electronic interactions between the iron ions and minor structural reorganization by changing the redox state.[66] The separations in $E°'$ value of consecutive ET processes ($\Delta E°'$) are large (0.266 V, 0.219 V and 0.315 V with increasing oxidation state) and reflect the stabilization energy imparted to the complex by electron delocalization.[67,68]

The $\Delta E°'$ values correspond to rather large comproportionation constants ($K_c = \exp[nF(E°_1–E°_2)/RT]$)[69,70] ranging between 10^4 and 10^6. This indicates high thermodynamic stability of the redox-active forms of the complex toward disproportionation (Table 3) and suggests the possibility of isolating a pure solid mixed-valence compound from its solution.[71] The negative $E°'$ values are comparable to those found for other related iron-complexes.[54,72]

The heterogeneous ET rate constant k_{ET} decreases with increasing oxidation state (and charge) of the complex (Table 3). This could be related to a progressive increase in the reorganization energy λ, as already observed for other mixed valence complexes.[73]

Table 3. Electrochemical data from CV for the subsequent ET processes of **2** in dichloromethane at −10 °C, using TBACl 0.1 M as base electrolyte.

	$E°'$/V [(a)]	$\Delta E°'$/V [(b)]	K_c [(c)]	k_{ET}/cm s^{-1} [(d)]
E(I)	−1.117			0.00444
		0.266	$1.26 \cdot 10^5$	
E(II)	−0.851			0.00364
		0.219	$1.58 \cdot 10^4$	
E(III)	−0.632			0.00253
		0.315	$1.10 \cdot 10^6$	
E(IV)	−0.317			0.00212

(a) $E°'$ = formal reduction potential. (b) $\Delta E°'$ = separation in $E°'$ values of subsequent ET processes. (c) K_c = comproportionation constant. (d) k_{ET} = heterogeneous ET rate constant.

Magnetic studies. DC magnetic measurements, performed on crystalline $\mathbf{2} \cdot 2.6CH_2Cl_2 \cdot 0.84Et_2O$, are presented in Figure 5 as a $\chi_M T$ vs T plot (χ_M is molar magnetic susceptibility). They provide a room-temperature $\chi_M T$ value of 16.6 emu·K·mol^{-1}, significantly larger than the cumulative Curie constant for four high-spin (S = 2) iron(II) ions (C_{tot} ~ 12 emu·K·mol^{-1} with g = 2.00). Such a difference can be ascribed to either orbital momentum or dominant ferromagnetic coupling. An initial smooth increase of $\chi_M T$ upon cooling is followed by a fast decrease below ~ 100 K, with $\chi_M T$ = 4.8 emu·K·mol^{-1} at 2 K. This suggests that antiferromagnetic coupling or magnetic anisotropy effects become important at low temperature. The presence of a weakly-magnetic ground state is confirmed by low temperature M_M vs H data (Figure 5, inset). The magnetization increases slowly upon increasing field and the largest measured magnetization (~8 $N_A\mu_B$ at 5 T and 2 K) is only about 50% of the expected saturation value (~ 16 $N_A\mu_B$ with $g = 2.00$).

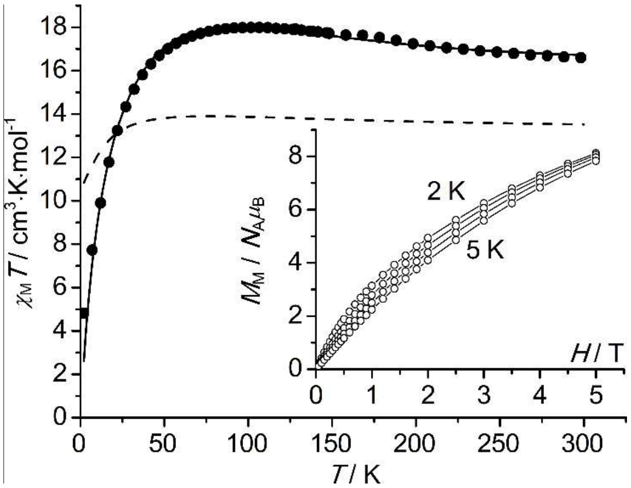

Figure 5. Magnetic properties of **2**·2.6CH$_2$Cl$_2$·0.84Et$_2$O as $\chi_M T$ vs T plot measured at 1 kOe (main panel, every fifth data point displayed) and M_M vs H plot at 2, 3, 4 and 5 K (inset). The dashed line in the main panel shows the magnetic response of the four anisotropic non-interacting iron(II) ions (see text), with all ligand field parameters held fixed at the values resulting from AOM calculations. The solid line was calculated with the best-fit parameters reported in the text. The solid lines in the inset are a guide to the eye.

To get insight into the observed magnetic behavior, we performed ligand-field calculations on the four iron(II) ions within the AOM, using the AOMX program package[40] (see Supporting Information for details). The two terminal metals (Fe1 and Fe4) possess close to trigonal pyramidal geometry and their ligand-field splitting is similar to that found in iron(II) pyrrolide complexes.[74-76] In exactly trigonal geometry the degenerate 3d_{xz} and 3d_{yz} orbitals lie lowest in energy, yielding a Jahn-Teller active ^5E ground term with unquenched orbital momentum. Spin-orbit interaction then causes a large magnetic anisotropy of the easy-axis type along the trigonal axis. Deviations from trigonal symmetry produce a splitting of the ^5E term and reduce the ground-state orbital momentum. However, in both Fe1 and Fe4 this splitting ($2\delta \sim$ 30-35 cm^{-1}) is sufficiently small (Table S4) compared with the effective spin-orbit coupling constant ($\zeta_{3\mathrm{d}} = 350\ \mathrm{cm}^{-1}$)[44] that its impact on calculated $\chi_M T$ vs T curves is negligible (see Figure S6).[76] Therefore, in all subsequent calculations axial symmetry (C_{3v}) was enforced on the $\mathrm{FeN_3Cl}$ chromophores, with average metrical parameters over Fe1 and Fe4. Next, using the PHI v3.0.6 software,[77] we determined the crystal-field Hamiltonian ($\widehat{H}_{CF,i}$) to be applied to the ^{5}D Russell-Saunders term of the terminal iron(II) ions (i = 1, 4) in order to account for the lowest 25 zero-field levels resulting from AOM calculations (Table S5 and Figure S7). In the complete Hamiltonian used to describe Fe1 and Fe4

$$\widehat{H}_i = \widehat{H}_{CF,i} + \lambda_i k_i \hat{\mathbf{L}}_i \cdot \hat{\mathbf{S}}_i + \mu_B \mathbf{B} \cdot \left(k_i \hat{\mathbf{L}}_i + g_e \hat{\mathbf{S}}_i\right) \tag{1}$$

$\mathbf{L}_i$ and $\mathbf{S}_i$ are the orbital ($L_i = 2$) and spin ($S_i = 2$) angular momenta, respectively, $\lambda_i = -\zeta_{3\mathrm{d}}/2S_i = -87.5\ \mathrm{cm}^{-1}$ is the multielectronic spin-orbit coupling constant, $\mathbf{B}$ is the applied magnetic field and k_i is the orbital reduction factor (taken as unity for consistency with ref.[44]).

The two remaining iron(II) ions (Fe2 and Fe3) have a much more distorted coordination environment, which suggests they may exhibit a quenched first-order orbital momentum. AOM calculations (see Supporting Information for details) confirmed the occurrence of a well-isolated spin quintet ($S_i = 2$) state (Table S6) whose Zeeman splitting is accurately described within a spin Hamiltonian formalism:

$$\widehat{H}_i = \hat{\mathbf{S}}_i \cdot \bar{\bar{D}}_i \cdot \hat{\mathbf{S}}_i + \mu_B \mathbf{B} \cdot \bar{\bar{g}}_i \cdot \hat{\mathbf{S}}_i \tag{2}$$

where $\bar{\bar{D}}_i$ and $\bar{\bar{g}}_i$ are the ZFS and the g tensors respectively for the two ions (i = 2, 3). From the AOM calculation, both Fe2 and Fe3 have negative and substantial ZFS ($|D_i| \sim$ 8-12 cm^{-1}), small-to-moderate rhombic distortion ($|E_i/D_i|$ = 0.03-0.13), $g_{\alpha,i}$ = 2.00-2.05 ($\alpha = x, y$) and $g_{z,i}$ = 2.17-2.22. Interestingly, the easy axis of Fe2 and Fe3 forms a large angle (92° and 104°) with the Fe2–Fe1 and Fe3–Fe4 directions, respectively, indicating the occurrence of markedly non-collinear magnetic anisotropies in the molecule

(Table S7). For simplicity, in all subsequent calculations both Fe2 and Fe3 were assumed to have axial anisotropy with D_i = –9.12 cm^{-1}, $g_{x,i}$ = $g_{y,i}$ = 2.033 and $g_{z,i}$ = 2.195 and their easy axes were taken orthogonal to the trigonal axes of the neighboring terminal ions.

The magnetic response calculated from these single-ion parameters assuming four uncoupled metal centers is shown in Figure 5 as a dashed curve. The large departures from the experimental data suggest that magnetic exchange interactions play an important role and DFT calculations were used as a general hint to their sign and magnitude. Considering eight broken-symmetry spin configurations, we found that the lowest-energy state has an up-up-down-down spin configuration for both NRLMOL and VASP, with ferromagnetic 1-2 and 3-4 interactions of similar magnitude. This result is consistent with the idealized twofold molecular symmetry observed in the solid state. We thus simplified the treatment and used only two independent exchange-coupling constants in Heisenberg-Dirac-Van-Vleck spin Hamiltonian:

$$\hat{H}_{HDVV} = J(\hat{\mathbf{S}}_1 \cdot \hat{\mathbf{S}}_2 + \hat{\mathbf{S}}_3 \cdot \hat{\mathbf{S}}_4) + J'\hat{\mathbf{S}}_2 \cdot \hat{\mathbf{S}}_3 \qquad (3)$$

which yielded J = –119.1 and J' = 2.2 cm^{-1} from the four lowest broken-symmetry spin configurations (results from NRLMOL). The ground spin state is thus generated by ferromagnetic 1-2 and 3-4 coupling and much weaker antiferromagnetic 2-3 coupling. Due to the inherent limitations of DFT, in which multi-configuration effects and self-interaction corrections are lacking, it is expected that these computed exchange couplings may be several times stronger than those from experimental data. For g = 2.00 they would in fact yield $\chi_M T$ = 18.9 emu·K·mol^{-1} at room temperature, which is close to the cumulative Curie constant for two S = 4 spins (C_{tot} = 20.0 emu·K·mol^{-1}) but distinctly larger than measured. Upon inclusion of orbital contributions, the calculated room-temperature $\chi_M T$ value would even more drastically exceed experimental data (Figure 5).

To account for exchange coupling in our treatment, we modeled **2** as a linear array composed of two identical ferromagnetic Fe_2 units (*i.e.* Fe1,Fe2 and Fe3,Fe4) weakly antiferromagnetically coupled with each other, as described by Hamiltonian:

$$\hat{H} = \hat{H}_{HDVV} + \sum_{i=1}^{4} \hat{H}_i \qquad (4)$$

where the $\hat{H}_i$'s are defined in Eq. (1) and (2). Intradimer exchange coupling (J) was introduced as an interaction between true spins (Lines' approach).[77,78] Because of the expectedly much weaker 2-3 coupling, the model was halved to include only one Fe_2 unit and interdimer interaction (J_{eff}) was treated in the mean-field approximation. Finally, for an accurate reproduction of high-temperature data a correction for TIP was introduced.[16,60] The resulting best-fit parameters (Figure 5) are $J = -21.4(4)$ cm^{-1}, $J_{\mathrm{eff}}/g_{av}^2 = 0.345(7)$ cm^{-1} and TIP = $2.1(2)\cdot10^{-3}$ emu mol^{-1}, where g_{av} is the average g-factor of the Fe_2 unit (assumed to be T-independent). The best-fit J value confirms that ferromagnetic coupling is present in **2**, albeit it is considerably weaker than predicted by DFT calculations. The ferromagnetic interaction is however one order of magnitude stronger than in dimeric compound **5**, which features a similar bridging motif.[60] It is also meaningful to compare **2** with diiron(II) compound **6**, which resembles each Fe_2 unit in **2** and indeed exhibits a similar tendency to parallel spin alignment.[16] In this case, however, a description of magnetic coupling in terms of localized spins is questionable due to the short Fe···Fe separation (2.29 Å) and delocalized metal-metal bonding.

In spite of the noncollinear anisotropies within the Fe1,Fe2 and Fe3,Fe4 pairs, the terminal iron(II) ions provide the largely dominant anisotropic contribution. Consequently each diiron(II) fragment has a huge easy-axis anisotropy, with a calculated susceptibility (at 2 K and 1 kOe) twenty-five times higher along the chain axis than orthogonal to it. Furthermore the small antiferromagnetic interdimer coupling is expected to lead to an array of low-lying excited states closely spaced in energy. Such a scenario and the prominent magnetic anisotropy, which is expected to lead to very extended spectra, may explain why the sample failed to give any detectable EPR signal (331.2 GHz and 441.6 GHz) in the temperature range from 10 to 30 K.

Given its magnetic anisotropy, **2** was tested for slow relaxation of the magnetization. AC magnetic measurements were thus performed on the same crystalline sample used for DC studies at temperatures down to 2 K and with a frequency (ν) of the 3 Oe oscillating magnetic field up to 1500 Hz. Since no out-of-phase component of the molar magnetic susceptibility (χ_M'') was detected in zero applied DC field, preliminary scans of χ_M'' vs ν were made at 2 K and different DC field values ranging from zero to 2.5 kOe. The results reveal the onset of slow relaxation of the magnetization above 500 Oe, with fields in the range 1.25-2.5 kOe leading to similar dynamic responses (Figure S8). A static field of 2 kOe was chosen to perform isothermal χ_M'' vs ν scans between 2.0 and 5.0 K. A non-zero χ_M'' was clearly observed below 2.8 K, where χ_M'' increases with increasing frequency (Figure S9). Since no maximum in the χ_M'' vs ν curves could be detected in the available frequency range, the temperature-dependent relaxation time could not be reliably extracted by fitting each curve to the (generalized) Debye model.[79,80] However, provided that only one characteristic relaxation process of the Debye type is present, with one energy barrier and one time constant, the relaxation parameters in the Arrhenius law $\tau = \tau_0\exp(U_{\mathrm{eff}} / k_BT)$ can be roughly evaluated using equation[81,82]

$$\ln(\chi_M''/\chi_M') = \ln(\omega\tau_0) + U_{\mathrm{eff}} / k_BT \qquad (5)$$

where $\omega = 2\pi\nu$ and χ_M' is the in-phase component of the molar magnetic susceptibility. Plotting $\ln(\chi_M''/\chi_M')$ vs $1/T$ and performing a linear regression at each frequency above $\nu = 65$ Hz (Figure S10) yielded $\tau_0 = 2.6(2.1) \times 10^{-7}$ s and $U_{\mathrm{eff}}/k_B = 10.1(1.3)$ K (the parameters are average values over frequency, and numbers in parentheses are the associated standard deviations). The similarity in ligand field splitting between the terminal iron(II) ions in **2** and iron(II) pyrrolide complexes, which behave as in-field single-molecule magnets,[74-76] suggests that the large magnetic anisotropy of Fe1 and Fe4 is likely at the origin of the out-of-phase response detected in **2**. One interesting result of our study is that slow magnetic relaxation persists notwithstanding the weak antiferromagnetic coupling between the two easy-axis diiron(II) units.

CONCLUSION

The wide class of EMACs supported by oligo-α-pyridylamido ligands, known since five decades,[2,3,10,83] was finally extended to include homometallic iron derivatives. Under strictly anaerobic and anhydrous condition, three tpda^{2-} ligands and two capping chlorides direct the formation of a chiral EMAC structure featuring four lined-up high-spin iron(II) centres. This compound proved sufficiently stable to be characterized by spectroscopic, electrochemical and magnetic techniques. CV measurements revealed a rich electrochemistry, with four quasi-reversible one-electron redox processes spanning a potential window of only 0.8 V. AOM calculations provided further insight into the electronic structure of the four iron(II) ions, pointing to significant differences between inner and terminal centres. While the heavily-distorted coordination geometry of the former quenches their first-order orbital angular momentum, the terminal ions reside in an approximately trigonal pyramidal environment and possess unquenched orbital momentum. Spin-orbit interaction then produces a large easy-axis magnetic anisotropy along their idealized trigonal axis, which is almost collinear with the chain axis. DFT studies and magnetic measurements coherently indicate that the molecule comprises two pairs of ferromagnetically-coupled iron(II) ions, weakly antiferromagnetically coupled with each other. In spite of such an interdimer coupling, slow magnetic relaxation was detected in AC susceptibility measurements, albeit only in the presence of a DC field and with an estimated energy barrier of only 10 K.

Building up from the foregoing results, we envision that a further strengthening of ferromagnetic interactions may follow from the incorporation of an additional $tpda^{2-}$ ligand and a fifth iron(II) ion in the structure.[19] The resulting $[Fe_5(tpda)_4Cl_2]$ complex, which would most probably be isostructural to its known Cr, Co, Ni and Ru congeners[1-3,65] and would contain Fe-Fe bonds, was occasionally detected in ESI-MS spectra but never isolated. An exciting alternative is partial chemical oxidation of **2**, a feasible process according to our CV studies. In fact, a mechanism of electronic interaction known as *double exchange* becomes operative in mixed-valent systems and generally provides a very effective source of ferromagnetic coupling between ions in different oxidation states.[84-86] Work in both directions is currently underway to enforce thermally-persistent high-spin states in iron-based EMACs.

ASSOCIATED CONTENT

Supporting Information

The Supporting Information is available free of charge on the ACS Publications website at DOI: XXX

ESI-MS, UV-Vis-NIR and NMR spectra, optical picture of the crystals, additional crystallographic information, listing of interatomic distances and angles, results of BVS calculations, details on AOM calculations and on EPR and AC magnetic measurements (PDF)

Accession Codes

CCDC 1819728 contains the supplementary crystallographic data for this paper. These data can be obtained free of charge via www.ccdc.cam.ac.uk/data_request/cif, or by emailing data_request@ccdc.cam.ac.uk, or by contacting The Cambridge Crystallographic Data Centre, 12 Union Road, Cambridge CB 1EZ, UK; fax: +44 1223 336033.

AUTHOR INFORMATION

Corresponding Author

* Email: acornia@unimore.it

Author Contributions

The manuscript was written through contributions of all authors. All authors have given approval to the final version of the manuscript.

Notes

The authors declare no competing financial interest.

ACKNOWLEDGMENT

This work was in part financed by University of Modena and Reggio Emilia and Italian MIUR through FAR2014 (Fondo di Ateneo per la Ricerca 2014) and FIRB (RBAP117RWN) projects, respectively. G. L. and K. P. were supported by the U.S. National Science Foundation grant No DMR-1206354. The computational support was provided by SDSC under DMR060009N and VT ARC computer clusters. A. C. and A. N. are grateful to A. Mucci (Department of Chemical and Geological Sciences) for stimulating discussion on NMR spectra.

ABBREVIATIONS

AC, alternating current; AOM, angular overlap model; CV, cyclic voltammetry; DC, direct current; DFT, density functional theory; EMAC, extended metal atom chain; ESI-MS, electrospray ionization mass spectrometry; ET, electron transfer; GC, glassy carbon; GGA, generalized gradient approximation; GOF, goodness of fit; Hdpa, 2,2'-dipyridylamine; Hhmds, 1,1,1,3,3,3-hexamethyldisilazane; HMes, mesitylene; H_2tpda, N^2,N^6-di(pyridin-2-yl)pyridine-2,6-diamine; LB, line broadening; NRLMOL, naval research laboratory molecular orbital library; PAR, Princeton applied research; PAW, projector-augmented-wave; PBE, Perdew-Burke-Ernzerhopf; H_3py_3tren, *N*,*N*,*N*-tris(2-(2-pyridylamino)ethyl)amine; SCE, saturated calomel electrode; SI, size of real spectrum; $TBABF_4$, tetra-*n*-butylammoniumtetrafluoborate; TBACl, tetra-*n*-butylammonium chloride; TD, size of fid; TIP, temperature-independent paramagnetism; VASP, Vienna Ab initio Simulation Package; ZFS, zero-field splitting.

REFERENCES

(1) Berry, J. F. Metal-Metal Bonds in Chains of Three or More Metal Atoms: From Homometallic to Heterometallic Chains. *Struct. Bonding* **2010**, *136*, 1–28.

(2) Hua, S.-A.; Cheng, M.-C.; Chen, C.; Peng, S.-M. From Homonuclear Metal String Complexes to Heteronuclear Metal String Complexes. *Eur. J. Inorg. Chem.* **2015**, *15*, 2510–2523.

(3) Hua, S.-A.; Tsai, Y.-C.; Peng, S.-M. A Journey of Metal-Metal Bonding beyond Cotton's Quadruple Bonds. *J. Chin. Chem. Soc.* **2014**, *61* (1), 9–26.

(4) Tanaka, Y.; Kiguchi, M.; Akita, M. Inorganic and Organometallic Molecular Wires for Single-Molecule Devices. *Chem. - Eur. J.* **2017**, *23* (20), 4741–4749.

(5) Chen, P.-J.; Sigrist, M.; Horng, E.-C.; Lin, G.-M.; Lee, G.-H.; Chen, C.; Peng, S.-M. A Ligand Design with a Modified Naphthyridylamide for Achieving the Longest EMACs: The 1st Single-Molecule Conductance of an Undeca-Nickel Metal String. *Chem. Commun.* **2017**, *53* (34), 4673–

4676.

(6) Ting, T.-C.; Hsu, L.-Y.; Huang, M.-J.; Horng, E.-C.; Lu, H.-C.; Hsu, C.-H.; Jiang, C.-H.; Jin, B.-Y.; Peng, S.-M.; Chen, C. Energy-Level Alignment for Single-Molecule Conductance of Extended Metal-Atom Chains. *Angew. Chem., Int. Ed.* **2015**, *54* (52), 15734–15738.

(7) Georgiev, V. P.; Mohan, P. J.; DeBrincat, D.; McGrady, J. E. Low-Symmetry Distortions in Extended Metal Atom Chains (EMACs): Origins and Consequences for Electron Transport. *Coord. Chem. Rev.* **2013**, *257* (1), 290–298.

(8) Cornia, A.; Rigamonti, L.; Boccedi, S.; Clérac, R.; Rouzières, M.; Sorace, L. Magnetic Blocking in Extended Metal Atom Chains: A pentachromium(II) Complex Behaving as a Single-Molecule Magnet. *Chem. Commun.* **2014**, *50* (96), 15191–15194.

(9) Christian, J. H.; Brogden, D. W.; Bindra, J. K.; Kinyon, J. S.; van Tol, J.; Wang, J.; Berry, J. F.; Dalal, N. S. Enhancing the Magnetic Anisotropy of Linear Cr(II) Chain Compounds Using Heavy Metal Substitutions. *Inorg. Chem.* **2016**, *55* (13), 6376–6383.

(10) Brogden, D. W.; Berry, J. F. Coordination Chemistry of 2,2'-Dipyridylamine: The Gift That Keeps on Giving. *Comments Inorg. Chem.* **2016**, *36* (1), 17–37.

(11) Craig, G. A.; Murrie, M. 3d Single-Ion Magnets. *Chem. Soc. Rev.* **2015**, *44* (8), 2135–2147.

(12) Cotton, F. A.; Daniels, L. M.; Falvello, L. R.; Matonic, J. H.; Murillo, C. A. Trigonal-lantern Dinuclear Compounds of Diiron(I,II): the Synthesis and Characterization of Two Highly Paramagnetic Fe_2(amidinato)$_3$ Species with Short Metal-metal Bonds. *Inorg. Chim. Acta* **1997**, *256*, 269–275.

(13) Cotton, F. A.; Daniels, L. M.; Matonic, J. H.; Murillo, C. A. Highly Distorted Diiron(II, II) Complexes Containing Four Amidinate Ligands. A Long and a Short Metal-metal Distance. *Inorg. Chim. Acta* **1997**, *256*, 277–282.

(14) L. Fohlmeister, S. Liu, C. Schulten, B. Moubaraki, A. Stasch, J. D. Cashion, K. S. Murray, L. Gagliardi, C. Jones, Low-Coordinate Iron(I) and Manganese(I) Dimers: Kinetic Stabilization of an Exceptionally Short Fe-Fe Multiple Bond. *Angew. Chem. Int. Ed.* **2012**, *51*, 8294–8298.

(15) Zall, C. M.; Zherebetskyy, D.; Dzubak, A. L.; Bill, E.; Gagliardi, L.; Lu, C. C. A Combined Spectroscopic and Computational Study of a High-Spin $S = 7/2$ Diiron Complex with a Short Iron–Iron Bond. *Inorg. Chem.* **2012**, *51* (1), 728–736.

(16) Tereniak, S. J.; Carlson, R. K.; Clouston, L. J.; Young, V. G., Jr.; Bill, E.; Maurice, R.; Chen, Y.-S.; Kim, H. J.; Gagliardi, L.; Lu, C. C. Role of the Metal in the Bonding and Properties of Bimetallic Complexes Involving Manganese, Iron, and Cobalt. *J. Am. Chem. Soc.* **2014**, *136*, 1842–1855.

(17) Hernández Sánchez, R.; Betley, T. A. Meta-Atom Behavior in Clusters Revealing Large Spin Ground States. *J. Am. Chem. Soc.* **2015**, *137* (43), 13949–13956.

(18) Hernández Sánchez, R.; Bartholomew, A. K.; Powers, T. M.; Ménard, G.; Betley, T. A. Maximizing Electron Exchange in a [Fe_3] Cluster. *J. Am. Chem. Soc.* **2016**, *138* (7), 2235–2243.

(19) Szarek, P.; Wegner, W.; Grochala, W. Ferromagnetic Ground State for a Hypothetical Iron-Based Extended Metal Atom Chain. *J. Mol. Model.* **2016**, *22* (3), 63.

(20) Nippe, M.; Berry, J. F. Introducing a Metal−Metal Multiply Bonded Group as an “Axial Ligand” to Iron: Synthetic Design of a Linear Cr−Cr···Fe Framework. *J. Am. Chem. Soc.* **2007**, *129* (42),

12684–12685.

(21) Nippe, M.; Wang, J.; Bill, E.; Hope, H.; Dalal, N. S.; Berry, J. F. Crystals in Which Some Metal Atoms Are More Equal Than Others: Inequalities From Crystal Packing and Their Spectroscopic/Magnetic Consequences. *J. Am. Chem. Soc.* **2010**, *132* (40), 14261–14272.

(22) Nippe, M.; Bill, E.; Berry, J. F. Group 6 Complexes with Iron and Zinc Heterometals: Understanding the Structural, Spectroscopic, and Electrochemical Properties of a Complete Series of M≡M···M′ Compounds. *Inorg. Chem.* **2011**, *50* (16), 7650–7661.

(23) Nippe, M.; Turov, Y.; Berry, J. F. Remote Effects of Axial Ligand Substitution in Heterometallic Cr ≡ Cr···M Chains. *Inorg. Chem.* **2011**, *50* (21), 10592–10599.

(24) Turov, Y.; Berry, J. F. Synthesis, Characterization and Thermal Properties of Trimetallic N_3–Cr≡Cr···M–N_3 Azide Complexes with M = Cr, Mn, Fe, and Co. *Dalton Trans.* **2012**, *41* (26), 8153–8161.

(25) Cotton, F. A.; Murillo, C. A.; Wang, X. Trinuclear Complexes of Copper, Cobalt and Iron with *N*,*N*′-di(2-Pyridyl) Formamidinate Ligands, $[M_3(DPyF)_4][PF_6]_2$. *Inorg. Chem. Commun.* **1998**, *1* (8), 281–283.

(26) Do, L. H.; Lippard, S. J. Toward Functional Carboxylate-Bridged Diiron Protein Mimics: Achieving Structural Stability and Conformational Flexibility Using a Macrocylic Ligand Framework. *J. Am. Chem. Soc.* **2011**, *133* (27), 10568–10581.

(27) Klose, A.; Solari, E.; Floriani, C.; Chiesi-Villa, A.; Rizzoli, C.; Re, N. Magnetic Properties Diagnostic for the Existence of Iron(II)-Iron(II) Bonds in Dinuclear Complexes Which Derive from Stepwise Insertion Reactions on Unsupported Iron-Aryl Bonds. *J. Am. Chem. Soc.* **1994**, *116*

(20), 9123–9135.

(28) Armarego, W. L. F. *Purification of Laboratory Chemicals*, 5th ed.; Elsevier, Ed.; Butterworth-Heinemann: Burlington, United States, 2003.

(29) Zhao, H.; Clérac, R.; Sun, J.-S.; Ouyang, X.; Clemente-Juan, J. M.; Gomez-Garcia, C. J.; Coronado, E.; Dunbar, K. R. A Comparative Structural and Magnetic Study of Three Compounds Based on the Cluster Unit $M_4Cl_8(THF)_6$ (M=Mn, Fe, Co). *J. Solid State Chem.* **2001**, *159* (2), 281–292.

(30) Dirvanauskas, A.; Galavotti, R.; Lunghi, A.; Nicolini, A.; Roncaglia, F.; Totti, F.; Cornia, A. Solution Structure of a Pentachromium(II) Single Molecule Magnet from DFT Calculations, Isotopic Labelling and Multinuclear NMR Spectroscopy. *Dalton Trans.* **2018**, *47*, 585–595.

(31) Bruker (2008). *APEX2*, *SADABS*, *SAINT*. Bruker AXS Inc., Madison, Wisconsin, USA.

(32) Altomare, A.; Cascarano, G.; Giacovazzo, C.; Guagliardi, A. Completion and Refinement of Crystal Structures with SIR 92. *J. Appl. Crystallogr.* **1993**, *26* (3), 343–350.

(33) Sheldrick, G. M. Crystal structure refinement with SHELXL. *Acta Crystallogr., Sect. C: Struct. Chem.* **2015**, *71* (1), 3–8.

(34) Farrugia, L. J. WinGX and ORTEP for Windows : An Update. *J. Appl. Crystallogr.* **2012**, *45* (4), 849–854.

(35) Thorn, A.; Dittrich, B.; Sheldrick, G. M. Enhanced Rigid-Bond Restraints. *Acta Crystallogr., Sect. A: Found. Crystallogr.* **2012**, *68* (4), 448–451.

(36) Belèn Meneses, A.; Antonello, S.; Arévalo, M. C.; Maran, F. Double-Layer Correction for

Electron-Transfer Kinetics at Glassy Carbon and Mercury Electrodes in *N*,*N*-Dimethylformamide. *Electroanalysis* **2006**, *18* (4), 363–370.

(37) Antonello, S.; Arrigoni, G.; Dainese, T.; De Nardi, M.; Parisio, G.; Perotti, L.; René, A.; Venzo, A.; Maran, F. Electron Transfer through 3D Monolayers on Au_{25} Clusters. *ACS Nano* **2014**, *8* (3), 2788–2795.

(38) Nicholson, R. S. Theory and Application of Cyclic Voltammetry for Measurement of Electrode Reaction Kinetics. *Anal. Chem.* **1965**, *37* (11), 1351–1355.

(39) Bain, G. A.; Berry, J. F. Diamagnetic Corrections and Pascal's Constants. *J. Chem. Educ.* **2008**, *85* (4), 532–536.

(40) Adamsky, H. with contributions from Hoggard, P. E.; Atanasov, M.; Eifert, K. *AOMX*, http://www.aomx.de (accessed February 2018).

(41) Bencini, A.; Benelli, C.; Gatteschi, D. The Angular Overlap Model for the Description of the Paramagnetic Properties of Transition Metal Complexes. *Coord. Chem. Rev.* **1984**, *60*, 131–169.

(42) Long, G. J.; Clarke, P. J. Crystal and Molecular Structures of *trans*-Tetrakis(pyridine)dichloroiron(II), -nickel(II), and -cobalt(II) and *trans*-Tetrakis(pyridine)dichloroiron(II) Monohydrate. *Inorg. Chem.* **1978**, *17* (6), 1394–1401.

(43) Little, B. F.; Long, G. J. Mössbauer, Electronic, and Structural Properties of Several Bis- and Tetrakis(pyridine)iron(II) Complexes. *Inorg. Chem.* **1978**, *17* (12), 3401–3413.

(44) Gerloch, M.; McMeeking, R. F.; White, A. M. Paramagnetic Ellipsoids and π Bonding in Dithiocyanatotetrapyridine-cobalt(II) and -iron(II). *J. Chem. Soc., Dalton Trans.* **1975**, *22*, 2452–

2459.

(45) Lever, A. B. P. *Inorganic Electronic Spectroscopy*, 2nd ed.; Elsevier, Ed.; Amsterdam, NY, 1984.

(46) Pederson, M. R.; Jackson, K. A. Variational Mesh for Quantum-Mechanical Simulations. *Phys. Rev. B* **1990**, *41* (11), 7453–7461.

(47) Jackson, K.; Pederson, M. R. Accurate Forces in a Local-Orbital Approach to the Local-Density Approximation. *Phys. Rev. B* **1990**, *42* (6), 3276–3281.

(48) Porezag, D.; Pederson, M. R. Optimization of Gaussian Basis Sets for Density-Functional Calculations. *Phys. Rev. A* **1999**, *60* (4), 2840–2847.

(49) Kresse, G.; Hafner, J. Ab Initio Molecular Dynamics for Liquid Metals. *Phys. Rev. B* **1993**, *47* (1), 558–561.

(50) Kresse, G.; Furthmüller, J. Efficient Iterative Schemes for Ab Initio Total-Energy Calculations Using a Plane-Wave Basis Set. *Phys. Rev. B* **1996**, *54* (16), 11169–11186.

(51) Perdew, J. P.; Burke, K.; Ernzerhof, M. Generalized Gradient Approximation Made Simple. *Phys. Rev. Lett.* **1996**, *77* (18), 3865–3868.

(52) Blöchl, P. E. Projector Augmented-Wave Method. *Phys. Rev. B* **1994**, *50* (24), 17953–17979.

(53) Kresse, G.; Joubert, D. From Ultrasoft Pseudopotentials to the Projector Augmented-Wave Method. *Phys. Rev. B* **1999**, *59* (3), 1758–1775.

(54) Zhao, Q.; Harris, T. D.; Betley, T. A. $[(^{H}L)_2Fe_6(NCMe)_m]^{n+}$ ($m = 0, 2, 4, 6$; $n = -1, 0, 1, 2, 3, 4, 6$): An Electron-Transfer Series Featuring Octahedral Fe_6 Clusters Supported by a Hexaamide

Ligand Platform. *J. Am. Chem. Soc.* **2011**, *133* (21), 8293–8306.

(55) Sundberg, J.; Vad, M. S.; McGrady, J. E.; Björemark, P. M.; Håkansson, M.; McKenzie, C. J. Accessing Iron Amides from Dimesityliron. *J. Organomet. Chem.* **2015**, *786*, 40–47.

(56) Tsao, T.-B.; Lo, S.-S.; Yeh, C.-Y.; Lee, G.-H.; Peng, S.-M. Novel Multi-Spin-State Linear Hexanickel Complexes Ni_6^{11+} and Their Singly Oxidized Products Ni_6^{12+} with 1,8-Naphthyridine-Based Ligands: Tuning the Redox Properties of the Metal String. *Polyhedron* **2007**, *26* (14), 3833–3841.

(57) Shieh, S.-J.; Chou, C.-C.; Lee, G.-H.; Wang, C.-C.; Peng, S.-M. Linear Pentanuclear Complexes Containing a Chain of Metal Atoms:$[Co_5^{II}(\mu_5\text{-tpda})_4(NCS)_2]$ and $[Ni_5^{II}(\mu_5\text{-tpda})_4Cl_2]$. *Angew. Chem., Int. Ed. Engl.* **1997**, *36* (12), 56–59.

(58) Ho, K.-Y.; Yu, W.-Y.; Cheung, K.-K.; Che, C.-M. Blue Luminescent zinc(II) Complexes with Polypyridylamine Ligands: Crystal Structures and Luminescence Properties. *J. Chem. Soc., Dalton Trans.* **1999**, *14* (10), 1581–1586.

(59) Brese, N. E.; O'Keeffe, M. Bond-Valence Parameters for Solids. *Acta Crystallogr., Sect. B: Struct. Sci.* **1991**, *47* (2), 192–197.

(60) Maddock, L. C. H.; Borilovic, I.; McIntyre, J.; Kennedy, A. R.; Aromí, G.; Hevia, E. Synthetic, Structural and Magnetic Implications of Introducing 2,2′-Dipyridylamide to Sodium-Ferrate Complexes. *Dalton Trans.* **2017**, *46* (20), 6683–6691.

(61) Cotton, F. A.; Daniels, L. M.; Murillo, C. A.; Wang, X. Getting the Right Answer to a Key Question Concerning Molecular Wires. *Chem. Commun.* **1999**, *5* (24), 2461–2462.

(62) Yeh, C.-Y.; Chou, C.-H.; Pan, K.-C.; Wang, C.-C.; Lee, G.-H.; Su, Y. O.; Peng, S.-M. Linear Pentacobalt Complexes: Synthesis, Structures, and Physical Properties of Neutral and One-Electron Oxidation Compounds. *J. Chem. Soc., Dalton Trans* **2002**, *5* (13), 2670–2677.

(63) Wang, C.-C.; Lo, W.-C.; Chou, C.-C.; Lee, G.-H.; Chen, J.-M.; Peng, S.-M. Synthesis, Crystal Structures, and Magnetic Properties of a Series of Linear Pentanickel(II) Complexes: $[Ni_5(\mu_5\text{-}tpda)_4X_2]$ ($X = Cl^-$, CN^-, N_3^-, NCS^-) and $[Ni_5(\mu_5\text{-}tpda)_4(CH_3CN)_2]\text{-}(PF_6)_2$ ($tpda^{2-}$ = the Tripyridyldiamido Dianion). *Inorg. Chem.* **1998**, *37* (16), 4059–4065.

(64) Cotton, F. A.; Daniels, L. M.; Jordan, G. T.; Murillo, C. A.; Pascual, I. Structural Variations in the Ligands around a Simple Oxo-Centered Building Block, the Tetrahedral $[M_4O]^{6+}$ Unit, M = Mn and Fe. *Inorg. Chim. Acta* **2000**, *297* (1–2), 6–10.

(65) Yin, C.; Huang, G.-C.; Kuo, C.-K.; Fu, M.-D.; Lu, H.-C.; Ke, J.-H.; Shih, K.-N.; Huang, Y.-L.; Lee, G.-H.; Yeh, C.-Y.; Chen, C.; Peng, S.-M. Extended Metal-Atom Chains with an Inert Second Row Transition Metal: $[Ru_5(\mu_5\text{-}tpda)_4X_2]$ ($tpda^{2-}$ = Tripyridyldiamido Dianion, X = Cl and NCS). *J. Am. Chem. Soc.* **2008**, *130* (31), 10090–10092.

(66) Geiger, W. E.; Connelly, N. G. The Electron-Transfer Reactions of Polynuclear Organotransition Metal Complexes. *Adv. Organomet. Chem.* **1985**, *24*, 87–130.

(67) Daniel, C.; Hartl, H. Neutral and Cationic V^{IV}/V^{V} Mixed-Valence Alkoxo-Polyoxovanadium Clusters $[V_6O_7(OR)_{12}]^{n+}$ ($R = -CH_3, -C_2H_5$): Structural, Cyclovoltammetric and IR-Spectroscopic Investigations on Mixed Valency in a Hexanuclear Core. *J. Am. Chem. Soc.* **2005**, *127* (40), 13978–13987.

(68) Gagne, R. R.; Spiro, C. L. An Electrochemical Method for Measuring Electronic Delocalization

in Mixed-Valent Species. *J. Am. Chem. Soc.* **1980**, *102* (4), 1443–1444.

(69) Richardson, D. E.; Taube, H. Determination of E_2^0-E_1^0 in Multistep Charge Transfer by Stationary-Electrode Pulse and Cyclic Voltammetry: Application to Binuclear Ruthenium Ammines. *Inorg. Chem.* **1981**, *20* (4), 1278–1285.

(70) Santi, S.; Bisello, A.; Cardena, R.; Donoli, A. Key Multi(ferrocenyl) Complexes in the Interplay between Electronic Coupling and Electrostatic Interaction. *Dalton Trans.* **2015**, *44* (12), 5234–5257.

(71) Ludi, A. *Mixed-Valence Compounds: Theory and Applications in Chemistry, Physics, Geology, and Biology*; Brown, D. B., Ed.; D. Reidel Publishing Company: Dordrecht, Holland, 1980; Chapter 1, pp 25-48.

(72) Zhao, Q.; Betley, T. A. Synthesis and Redox Properties of Triiron Complexes Featuring Strong Fe-Fe Interactions. *Angew. Chem., Int. Ed.* **2011**, *50* (3), 709–712.

(73) Brodsky, C. N.; Hadt, R. G.; Hayes, D.; Reinhart, B. J.; Li, N.; Chen, L. X.; Nocera, D. G. In Situ Characterization of Cofacial Co(IV) Centers in Co_4O_4 Cubane: Modeling the High-Valent Active Site in Oxygen-Evolving Catalysts. *Proc. Natl. Acad. Sci. U. S. A.* **2017**, *114* (15), 3855–3860.

(74) Freedman, D. E.; Harman, W. H.; Harris, T. D.; Long, G. J.; Chang, C. J.; Long, J. R. Slow Magnetic Relaxation in a High-Spin Iron(II) Complex. *J. Am. Chem. Soc.* **2010**, *132* (4), 1224–1225.

(75) Harman, W. H.; Harris, T. D.; Freedman, D. E.; Fong, H.; Chang, A.; Rinehart, J. D.; Ozarowski, A.; Sougrati, M. T.; Grandjean, F.; Long, G. J.; Long, J. R.; Chang, C. J. Slow Magnetic Relaxation in a Family of Trigonal Pyramidal Iron(II) Pyrrolide Complexes. *J. Am. Chem. Soc.* **2010**, *132*

(51), 18115–18126.

(76) Atanasov, M.; Ganyushin, D.; Pantazis, D. A.; Sivalingam, K.; Neese, F. Detailed Ab Initio First-Principles Study of the Magnetic Anisotropy in a Family of Trigonal Pyramidal Iron(II) Pyrrolide Complexes. *Inorg. Chem.* **2011**, *50* (16), 7460–7477.

(77) Chilton, N. F.; Anderson, R. P.; Turner, L. D.; Soncini, A.; Murray, K. S. PHI: A Powerful New Program for the Analysis of Anisotropic Monomeric and Exchange-Coupled Polynuclear *d*- and *f*-Block Complexes. *J. Comput. Chem.* **2013**, *34* (13), 1164–1175.

(78) Lines, M. E. Orbital Angular Momentum in the Theory of Paramagnetic Clusters. *J. Chem. Phys.* **1971**, *55* (6), 2977–2984.

(79) Cole, K. S.; Cole, R. H. Dispersion and Absorption in Dielectrics I. Alternating Current Characteristics. *J. Chem. Phys.* **1941**, *9* (4), 341–351.

(80) Dekker, C.; Arts, A. F. M.; de Wijn, H. W.; van Duyneveldt, A. J.; Mydosh, J. A. Activated Dynamics in a Two-Dimensional Ising Spin Glass: $Rb_2Cu_{1-x}Co_xF_4$. *Phys. Rev. B* **1989**, *40* (16), 11243–11251.

(81) Bartolomé, J.; Filoti, G.; Kuncser, V.; Schinteie, G.; Mereacre, V.; Anson, C. E.; Powell, A. K.; Prodius, D.; Turta, C. Magnetostructural Correlations in the Tetranuclear Series of $\{Fe_3LnO_2\}$ butterfly core clusters: Magnetic and Mössbauer spectroscopic study. *Phys. Rev. B* **2009**, *80* (1), 14430.

(82) Langley, S. K.; Ungur, L.; Chilton, N. F.; Moubaraki, B.; Chibotaru, L. F.; Murray, K. S. Structure, Magnetism and Theory of a Family of Nonanuclear $Cu^{II}_5Ln^{III}_4$–Triethanolamine Clusters Displaying Single-Molecule Magnet Behaviour. *Chem. - Eur. J.* **2011**, *17* (33), 9209–9218.

(83) Hurley, T. J.; Robinson, M. A. Nickel(II)-2,2'-dipyridylamine System. I. Synthesis and Stereochemistry of the Complexes. *Inorg. Chem.* **1968**, *7* (1), 33–38.

(84) Drüeke, S.; Chaudhuri, P.; Pohl, K.; Wieghardt, K.; Ding, X.-Q.; Bill, E.; Sawaryn, A.; Trautwein, A. X.; Winkler, H.; Gurman, S. J. The Novel Mixed-valence, Exchange-coupled, Class III Dimer $[L_2Fe_2(\mu\text{-OH})_3]^{2+}$ (L = *N,N',N''*-Trimethyl-1,4,7-triazacyclononane). *J. Chem. Soc., Chem. Commun.* **1989**, 59–62.

(85) Gamelin, D. R.; Bominaar, E. L.; Kirk, M. L.; Wieghardt, K.; Solomon, E. I. Excited-state Contributions to Ground-state Properties of Mixed-valence Dimers: Spectral and Electronic-structural Studies of $[Fe_2(OH)_3(tmtacn)_2]^{2+}$ Related to the $[Fe_2S_2]^{+}$ Active Sites of Plant-Type Ferredoxins. *J. Am. Chem. Soc.* **1996**, *118*, 8085–8097.

(86) Gaudette, A. I.; Jeon, I.-R.; Anderson, J. S.; Grandjean, F.; Long, G. J.; Harris, T. D. Electron Hopping through Double-Exchange Coupling in a Mixed-Valence Diiminobenzoquinone-Bridged Fe_2 Complex. *J. Am. Chem. Soc.* **2015**, *137* (39), 12617–12626.

SYNOPSIS

Working under strictly inert conditions, the class of extended metal atom chains supported by oligo-α-pyridylamido ligands was finally extended to include homometallic iron(II) species. The elusive string-like complex [$Fe_4(tpda)_3Cl_2$] undergoes four quasi-reversible one-electron oxidations in dichloromethane solution and displays weak single-molecule magnet response in the solid state. Magnetic measurements and DFT calculations support the presence of two pairs of ferromagnetically coupled high-spin iron(II) ions, weakly antiferromagnetically coupled with each other.